Bulletin of the Seismological Society of America, Vol. 101, No. 5, pp. 2162–2175, October 2011, doi: 10.1785/0120100260

Basin Shear-Wave Velocities beneath Seattle, Washington, from Noise-Correlation Rayleigh Waves

by Andrew A. Delorey and John E. Vidale

Abstract Tomography with short-period Rayleigh waves, extracted using noise interferometry, can refine *S*-wave velocity (V_S) models in urban areas with dense arrays of short-period and broadband instruments. We apply this technique to the Seattle area to develop a new shallow V_S model for use in seismic-hazard assessment. Continuous data from the Seismic Hazards in Puget Sound (SHIPS) array and local broadband stations have interstation distances of 90 km or less. This spacing allows us to extract Rayleigh waves with periods between 2 and 10 s that are sensitive to shallow-basin structure.

This new V_S model for the Seattle basin is constructed using direct observations rather than using *P*-wave velocity (V_P) observations and a V_P/V_S ratio as all previous 3D models at this scale have been constructed. Our results reveal greater detail in the upper 3.5 km than previous models. Earthquake simulations calculated using our new model better predict peak ground velocities (PGV) at periods between 1 and 2 s for two local earthquakes than the previous model used to calculate Seattle's seismic-hazard map (Frankel *et al.*, 2007).

We collected data from two local earthquakes and ran finite-difference simulations using our new velocity model as well as the previous velocity model used in development of the Seattle seismic-hazard maps to assess how well our model predicts ground motions relative to the previous model. With a recent deployment of Netquakes strong-motion stations by the Pacific Northwest Seismic Network (PNSN) and the U.S. Geological Survey, we are now able to make more comprehensive assessments of the predictions for recent events.

Online Material: Cross sections of the shear-wave velocity model of the Seattle basin, with comparison to the 2D model of Snelson *et al.* (2007), and the digital shear-wave velocity model.

Introduction

Seattle, Washington, one of the largest cities in the United States that is threatened by earthquakes, sits atop a deep sedimentary basin. Nearby, Everett and Tacoma, Washington, have a similar setting. These basin structures are the result of the evolution of the Puget Lowland forearc basin, which combines strike-slip and thrust-fault earthquakes to accommodate right-lateral strike-slip and north–south shortening (Johnson *et al.*, 1996; Pratt *et al.*, 1997). The north–south shortening is driven by the oblique subduction of the Juan de Fuca plate under the North American plate (Riddihough, 1984). As a result, Cascadia, which comprises the region from northernmost California to southern British Columbia where the Juan de Fuca plate is subducting beneath North America, is being squeezed between the Sierra Nevada block and western Canada (Wells *et al.*, 1998; Wells and Simpson, 2001).

The Seattle basin is described in a number of papers (Pratt *et al.*, 1997; Brocher *et al.*, 2001; Blakely *et al.*, 2002; ten Brink *et al.*, 2002; ten Brink *et al.*, 2006, Fig. 1). The nearby Tacoma basin (Pratt *et al.*, 1997; Brocher *et al.*, 2001) and Everett basin (Johnson *et al.*, 1996) have also been studied but remain less well understood. The Kingston Arch separates the Seattle basin from the Everett basin, and the Seattle uplift separates the Seattle basin from the Tacoma basin (Fig. 1). In a series of studies in the past decade, models were developed for these basins because they are known to

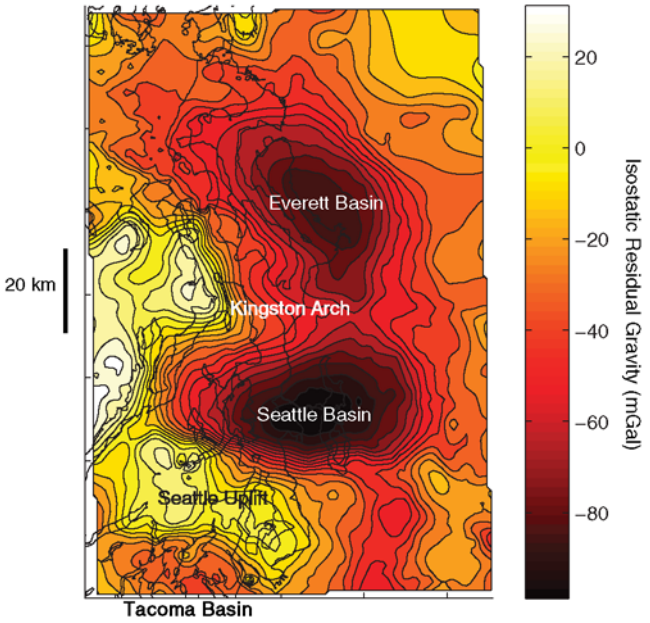

Figure 1. Geometry of basins as revealed by gravity variations around Seattle, Everett, and Tacoma, Washington (Brocher *et al.*, 2001). The color version of this figure is available only in the electronic edition.

amplify seismic shaking (Frankel *et al.*, 1999; Frankel *et al.*, 2002; Pratt, Brocher, *et al.*, 2003; Barberopoulou *et al.*, 2004; Brocher *et al.*, 2004). Many of the buildings in the region were constructed well before this recent characterization of the effects of basin amplification on seismic hazards.

The basins of the Puget lowland require study to improve modeling of three-dimensional features. The young unconsolidated deposits are a temporally and spatially complex stratigraphy of glacial outwash, till, lacustrine, and recessional deposits formed when the lowland was glaciated at least six different times in the Pleistocene (Booth, 1994). The top several kilometers are peppered with smaller-scale basins, and the deeper basins are likely delineated by the major bounding faults.

Seismic Hazards

Three types of earthquakes are known to occur in the Seattle area, as is typical for subduction zones:

- Most damaging for the urbanized areas are the shallow crustal events (ten Brink *et al.*, 2002; Haugerud *et al.*, 2003; Sherrod *et al.*, 2004) due in part to their close proximity. The most recent documented instance of a large event on the Seattle fault was the moment magnitude (M_w) 7.5 event in about 900 A.D. (ten Brink *et al.*, 2006), which featured 7 m of surface slip. There is also evidence of uplift in the vicinity of the Tacoma fault about 1000 yr ago (Bucknam *et al.*, 1992; Brocher *et al.*, 2001). Numerous other faults are present, and more are being found as geologists image the landscape with Light Detection and Ranging (LiDAR), but which faults are currently active and their recurrence intervals are not well known.
- M_w 9 megathrust events strike the Pacific Northwest coast roughly every 500 yr (Atwater, 1992; Goldfinger *et al.*, 2003; Satake *et al.*, 2003). These events may produce strong long-period basin excitation lasting many minutes.
- Deep intraslab earthquakes within the subducting slab have been the most common in recent decades, with M_w 6.5 to M_w 6.8 events in 1949, 1965, and 2001 (Ichinose *et al.*, 2004; 2006).

Seismic hazards are commonly estimated by predicting the shaking at a rock site from vertically incident seismic waves using a local velocity model, and then performing a site response analysis to model the effect of unconsolidated soils on ground motions. However, the basins have an additional effect of focusing and trapping energy within them (Frankel *et al.*, 2002; Frankel *et al.*, 2007), which is not modeled with many traditional methods.

Some of the patterns of shaking have been captured with studies solely examining site amplification (Hartzell *et al.*, 2000). Site amplifications are commonly estimated for sites for which recordings have not been collected or analyzed based on nearby observations. For some sites, the back azimuth to an earthquake may have a strong influence. Recorded ground motions from both strong and weak shaking indicate patterns of amplification that vary with site location, source location, and frequency (Frankel *et al.*, 2002; Barberopoulou *et al.*, 2004).

Seismic-hazard maps rely heavily on the ability to predict ground motions for a wide variety of plausible earthquakes that have never been instrumentally observed (Frankel *et al.*, 1996; Frankel *et al.*, 2007). In Seattle's case, these unrecorded earthquakes include large crustal events (M_w 6.0–7.5) on faults in the Cascadia forearc including the Seattle fault, and a megathrust event ($> M_w$ 8.5) off the Pacific coast. In order to predict ground motions for these and other events, it is essential to have a good V_S model for the Seattle area.

Many existing local velocity models are sufficient for predicting ground motions at rock sites while modeling the effects of simple geological structures but are not sufficient to model the effects of more complex crustal and sedimentary structures like the Seattle basin. Prior to this study, there were no V_S models, based on direct observations, detailed enough to model the effects of the Seattle basin on ground motions at 1 Hz. The primary motivation of this study is to produce a V_S model detailed enough to make ground-motion predictions at 1 Hz within the Seattle basin, and we will evaluate our results based on this goal.

Previous Models

Earthquake tomography and active-source experiments have revealed the larger-scale features of the crust around Seattle (Lees and Crosson, 1990; Pratt *et al.*, 1997; Symons and Crosson, 1997; Van Wagoner *et al.*, 2002; Pitarka *et al.*,

2004) as well as northern Cascadia (Ramachandran *et al.*, 2004, 2005, 2006). Tomographic models indicate a Seattle basin structure that has a symmetrical bowl shape in the east–west direction and asymmetry in the north–south direction consistent with formation by motion along the Seattle fault (Fig. 1). These studies find a crustal thickness of 35 km (Schultz and Crosson, 1996) and provide a useful regional velocity model as a starting point for basin models, but do not have adequate resolution to model basin waves. Also, because they are mostly derived from short-period, vertical-component seismometers, *S* waves are difficult to reliably identify, and thus V_S models are less well constrained.

High-resolution basin models have been solely built on *P*-wave observations until the most recent work (Snelson *et al.*, 2007). This is a 2D west-to-east refraction profile across the basin, not a fully 3D model needed to make predictions for ground motions. The larger-scale V_S models are derived from the conversion of a V_P model through an assumed Poisson's ratio. Fluid content, porosity, and composition all affect Poisson's ratio, so a direct measurement of V_S is preferable. For velocities appropriate for sedimentary basins, data used to determine Brocher's (2005) empirical relationship between V_P and V_S are highly scattered. The V_P/V_S ratio is not simply a function of V_P for sedimentary rocks.

Important details remain unresolved (Snelson *et al.*, 2007). The thickness of the unconsolidated layers in recent models varies by up to a factor of 2, a problem in need of resolution. The inference of several shallow sub-basins would benefit from verification and further study. Attenuation, a critical parameter for estimates of ground shaking, has only been estimated from active-source experiments (Li *et al.*, 2006). Several different hypotheses exist for why the largest amplification peaks occur at stations above the deepest part of the Seattle basin; some of these hypotheses are the focusing of teleseismic energy by the serpentinized upper mantle or that the observed amplification is primarily controlled by unconsolidated sediments (Pratt, Brocher, *et al.*, 2003).

Model Calculation

We calculated the 3D V_S model in two steps. In the first step, we solved for the 2D Rayleigh-wave phase velocity model as a function of period between 2 and 10 s. The model space is 120 km east to west and 100 km north to south, centered on Seattle (Fig. 2). The velocity model was parameterized with an irregularly spaced grid with smaller spacing in regions with greater data coverage. Intergrid spacing ranged from 1 km near central Seattle to 20 km at the edges of the model. At each grid point, we used a third-order polynomial for phase velocity as a function of frequency. At each frequency and grid point, we calculated a Gaussian surface with a characteristic width equal to the square of the distance to the next closest grid point. The normalized sum of these surfaces determined the 2D velocity model at each frequency. We used a starting model that was a 1D average of the

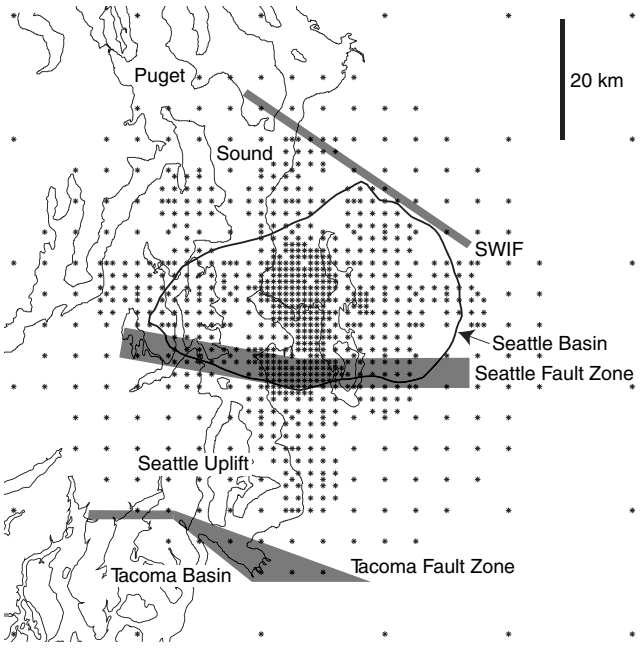

Figure 2. Parameter space for the phase velocity model. The asterisks indicate the locations of parameter nodes for the phase velocity model. The closed curve indicates the approximate boundary of the Seattle basin based on the gravity measurements of Brocher *et al.* (2001). The gray patches indicate the Seattle fault zone, Tacoma fault zone, and south Whidbey Island fault (SWIF) as labeled.

Stephenson (2007) model and two different forward calculations, ray theory and a single-scatterer approximation, to calculate the polynomial coefficients.

We inverted for the polynomial coefficients of the model using the following equation:

$$\mathbf{m} = (\mathbf{G}^T\mathbf{C}^{-1}\mathbf{G} + \gamma^2\mathbf{L}^T\mathbf{L})\mathbf{G}^T\mathbf{C}^{-1}\mathbf{d}.$$

$\mathbf{C}$ is the data covariance matrix, $\mathbf{G}$ is the partial derivative matrix, $\mathbf{L}$ is the normalization matrix, γ is a scaling parameter between goodness of fit and the normalization matrix, $\mathbf{d}$ is the data vector of observed phase velocities, and $\mathbf{m}$ is the model vector of polynomial coefficients.

In determining the data uncertainties for matrix $\mathbf{C}$, we estimated the uncertainties in calculating the Rayleigh-wave phase velocities. The most important source of error in our phase-velocity calculation was the way we augmented our dataset and solved the phase ambiguity using the model of Stephenson (2007). To test the error that would be introduced if our assumption that the phase velocity is 3.91 km/s at a 20 s period everywhere in the model space was incorrect, we considered other values. If we were off the actual phase velocity by 5% at a period of 20 s, the error introduced would only be about 2% at a period of 2 s, less for periods between 2 and 10 s. Another source of error comes from the possibility of phase shifting in the empirical Green's functions if the azimuthal distribution of coherent noise at the periods

we used was highly focused, though we did not find that to be the case. It was difficult to know for sure how much error was present, so we used a conservative estimate of 10% in our inversion.

The normalization matrix (**L**) is the sum of two different matrices. The first matrix is a diagonal matrix whose values were determined by the geographic location of the corresponding parameter. For each grid point, we calculated its mean distance to all of the stations, and used this as a proxy for the relative amount of data coverage. For points with a low mean distance, we gave a lower variance, and for stations with a high mean distance, we gave a higher variance. In this way, we were able to apply a greater penalty for perturbations to the starting model in regions with sparser data coverage. The second matrix measured the geographic roughness in the model using a finite-difference approximation of the curvature. With this matrix, we were able to apply a penalty for increasing roughness.

In order to estimate the effect of the starting model on our results, we ran this inversion using many different starting models. Beginning with our basic starting model, we added Gaussian noise with a standard deviation of 20% to all model nodes within the basin. We ran each of these models to a solution and then calculated the mean and standard deviation of the results. Within the basin, most regions showed a standard deviation of much less than 10%, with a few isolated spots as high as 15% where data coverage was sparse. This indicates that there is some dependence on the starting model mostly in the shallowest layers, but the variations were within our estimated uncertainties.

In the second step, we inverted the Rayleigh-wave dispersion curves for the 3D isotropic V_S structure. The horizontal dimensions are 60×60 km, centered on Seattle with uniform horizontal grid spacing of 2.5 km. The phase velocity model is bigger than the V_S model in order to include several stations outside the basin. However, for the V_S inversion, it was no longer necessary that those stations lie within the model, so we omitted parts of the model with the poorest data coverage. The vertical extent of the model was 160 km in depth in order to avoid any boundary problems with the forward problem; however, the Rayleigh-wave frequencies used, we estimate, were most sensitive to the top ~4 km of the model. Between 4- and 9-km depths, velocities were highly smoothed in part because we assigned higher penalties for roughness and deviation from the starting model at these depths and below. The grid spacing in the upper 10 km of the model ranges from 0.25 to 1 km, and the spacing size increases with depth through the rest of the model. We considered inclusion of a water layer for Puget Sound and Lake Washington, but at periods of 2 s and greater, the effect of the water layer for the relevant depths was only about 1% and only in very localized places.

We used a starting model based on Stephenson (2007) and calculated synthetic dispersion curves in our forward calculation using the method of Takeuchi and Saito (1972). We used a full 3D inversion so that we could apply normalization to the model as a whole. Our V_S inversion was similar to our phase-velocity inversion described in the previous paragraph. We used two normalization matrices: one is a Laplacian matrix that allowed us to apply a penalty for increasing roughness and the other is a parameter-variance matrix that allowed us to penalize perturbations to model parameters that represented regions not well constrained by the data. In particular, we assigned high variances to parameters deeper than 9 km because that is below the bottom of the Seattle basin, where we had little constraints from our data. As in the first inversion, we calculated solutions from a number of starting models perturbed by adding Gaussian noise to our original starting model. This time, the standard deviation of the noise was 5%, and the same noise was added to all points in a column. We used smaller levels of noise than with our phase-velocity calculations because adding higher levels of noise could have led to the generation of physically unrealistic velocity structures, which cause problems with the forward calculations. The resulting suite of models has a standard deviation of only about 1%, except in the uppermost layer.

Data

Most of our data came from the Seattle SHIPS array (Pratt, Meagher, *et al.*, 2003), with some additional data from stations around Seattle from the Pacific Northwest Seismic Network (PNSN) and Earthscope's Transportable Array (TA; see Fig. 3). During the Seattle SHIPS experiment, seismometers were deployed at 87 sites in a 110-km-long east–west line, three north–south lines, and a grid throughout the Seattle urban area from January to May 2002. Each site recorded three components of velocity using a 2-Hz L-22 sensor recording 50 samples per second. The PNSN and TA sites

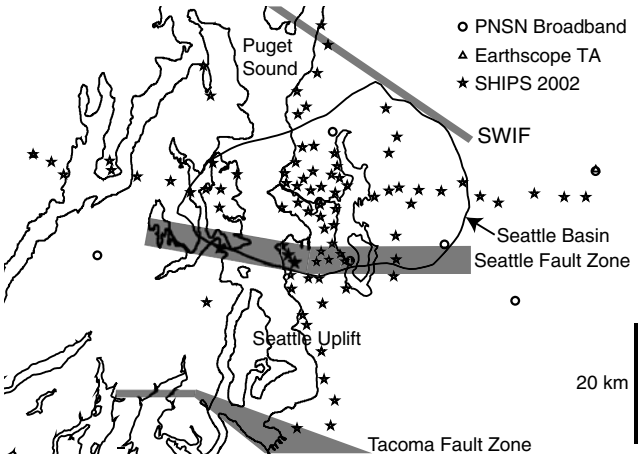

Figure 3. Stations used for this study. The closed curve indicates the approximate boundary of the Seattle basin based on the gravity measurements of Brocher *et al.* (2001). The gray patches indicate the Seattle fault zone, Tacoma fault zone, and south Whidbey Island fault (SWIF) as labeled. The circles indicate broadband stations of the PNSN, triangles indicate broadband stations of the Earthscope's TA, and stars indicate stations of the 2002 SHIPS array.

had three-component broadband Streckeisen STS-2, Guralp CMG-40T, or Guralp CMG-3T sensors recording 40 samples per second.

The L-22 sensor is a short-period instrument; however, we were able to determine Rayleigh-wave group velocities out to periods of 10 s or more in some cases by careful selection and processing of the data. Each instrument was individually calibrated during the SHIPS experiment, and we used the individual calibrations to deconvolve the instrument response, eliminating most of the variability in response among the instruments. According to the calibrations, the velocity sensitivity was on the order of 100 times higher at a period of 1 s than at a period of 10 s. Still, the amplitude of coherent energy at a period of 10 s was often high enough to observe a good Rayleigh-wave signal. We whitened the spectrum before bandpass filtering to ensure the proper frequency content in each wavelet despite frequency-dependent instrument sensitivity.

To extract Rayleigh wave wavelets, the vertical-component seismograms from all stations were merged and then cut to day-long segments. The instrument response was deconvolved, the signal was integrated to displacement, and the data downsampled to 10 samples per second. The cross correlations were computed as in Bensen *et al.* (2007). We used one-bit amplitude normalization because it produced cleaner and more prominent Rayleigh-wave wavelets than other amplitude normalization methods. Many station pairs were discarded if the station distance was not sufficiently large relative to the wavelength of the surface wave. Though we did not use a specific distance cutoff, we used only well-formed surface-wave wavelets. We used an automated system to discard the worst traces and manually evaluated the rest. Due to our selectivity in picking only the best data, we used only 13% of the possible paths. Two examples of band-passed empirical Green's functions are shown in Figure 4. In these two examples, noise coherence is very good from 10 s down to 2–3 s.

We first calculated the group velocity dispersion curve of each trace, starting at the longest period available, by calculating and selecting the peak of the envelope function. Traces that did not have coherence to at least 10-s periods were discarded. When we could not obtain the group-velocity dispersion up to a period of 20 s, which occurred in most of our paths, we extrapolated the curve by using group-velocity measurements calculated from the velocity model of Stephenson (2007). By applying a band-pass filter in small increments to our waveforms, we were able to track the peak of the envelope function to shorter periods, often down to between 2 and 3 s. We terminated our group velocity curve when the signal-to-noise ratio fell below 11.5 dB or if the peak of the envelope function jumped, split, or was otherwise ambiguous to track. The evaluation criteria were defined to select the most promising dispersion curves, which we then evaluated visually. The paths used are shown in Figure 5.

As described in Bensen *et al.* (2007), an additional constraint was needed to resolve the phase ambiguity associated

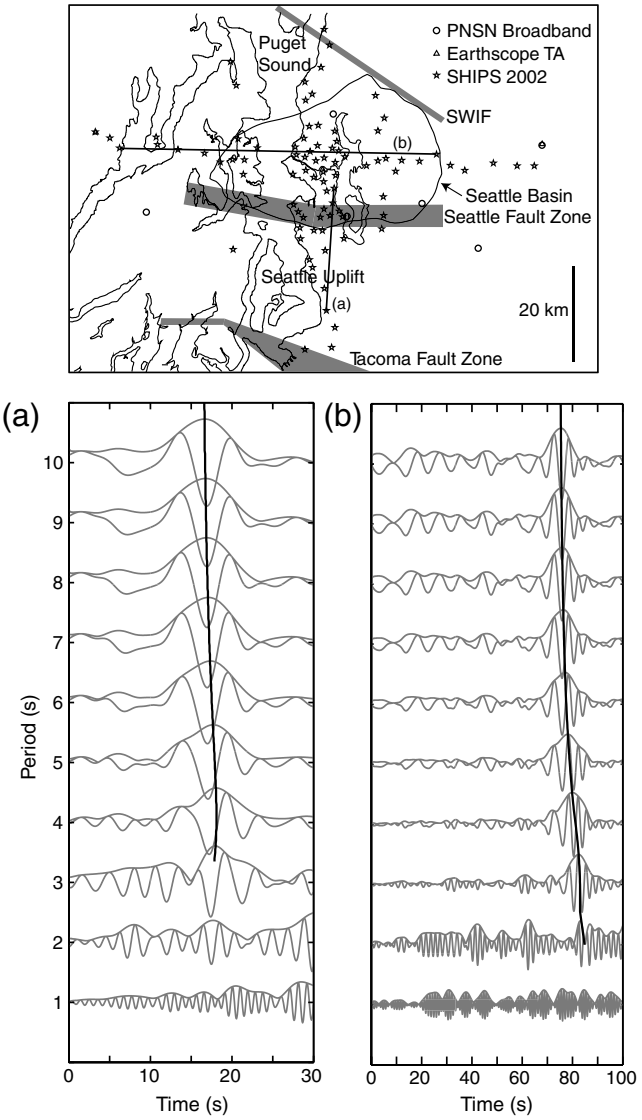

Figure 4. Two examples of empirical Green's functions band-pass filtered between 1- and 10-s periods. The two paths shown on the station map at the top are labeled (a) and (b) and correspond with the band-passed waveforms shown below.

with the calculation of surface-wave phase velocities from group velocities. To solve this ambiguity, we calculated Rayleigh-wave phase velocity dispersion curves for a uniform grid of 1D profiles taken from the V_S model of Stephenson (2007), using the method of Takeuchi and Saito (1972). Throughout the model, the calculated phase-velocity dispersion curves converge to ~3.91 km/s at a period of 20 s, indicating a nearly 1D velocity structure beneath the Seattle basin, in other words, depths below 9 km. Calculated phase velocities ranged from 1 to 2.25 km/s at a period of 1 s, indicating that velocities at basin depths vary laterally. We assumed that the Rayleigh-wave phase velocity is 3.91 km/s at a period of 20 s everywhere beneath the Seattle basin and integrated the group velocity curve from 20 s down to 2 s to determine phase velocities at these shorter periods.

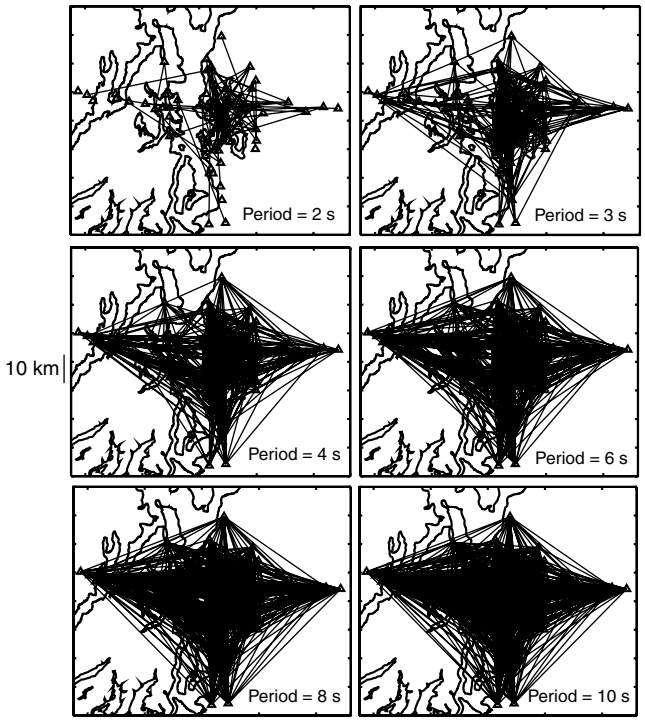

Figure 5. Lines represent paths for Rayleigh waves used to image the Seattle basin. The period is indicated at the lower right of each panel. Triangles represent stations of the SHIPS array.

The group velocity curve between 20 and 10 s was based on a combination of values from the model of Stephenson (2007) and from our cross correlations. The group velocity curve between 10 and 2 s was based exclusively on our cross correlations. In this fashion, we resolved the phase ambiguity and calculated the phase velocity dispersion curve from the group velocity dispersion curve using the phase velocity at a period of 20 s as the constant of integration:

$$S_c(\omega) = \omega^{-1}\left(\int_{\omega_n}^{\omega} s_u(\omega)d\omega + \omega_n s_c^n\right),$$

in which s_u is the group slowness, s_c is the phase slowness, and n indicates a period of 20 s (Bensen *et al.*, 2007).

The SHIPS array was not designed for this kind of analysis, and the station layout is not ideal for surface-wave tomography. In order for velocities to be well resolved for a model parameter, there must be many independent observations of the region in the form of crossing-wave propagation paths. For most of the periods we used, there were many crossing ray paths near the center of the model corresponding to the city of Seattle (Fig. 5). Away from the center of the model, there were fewer crossing paths, and at its perimeter, there were almost none. The lack of crossing ray paths can lead to the smearing of velocity perturbations along a ray's path.

We performed a resolution test to examine the horizontal resolution of our dataset (Fig. 6). In this test, we started with a 1D model and then generated a checkerboard pattern of higher and lower velocities with a width of 4 km and a perturbation magnitude of ~5% from the 1D model. Due to our irregularly spaced grid, not every velocity perturbation has exactly the same magnitude. We generated synthetic data from this perturbed 1D model and then ran our inversion using the 1D model as a starting model. The misfit reduction after three iterations of our inversion was 98%. Our recovery

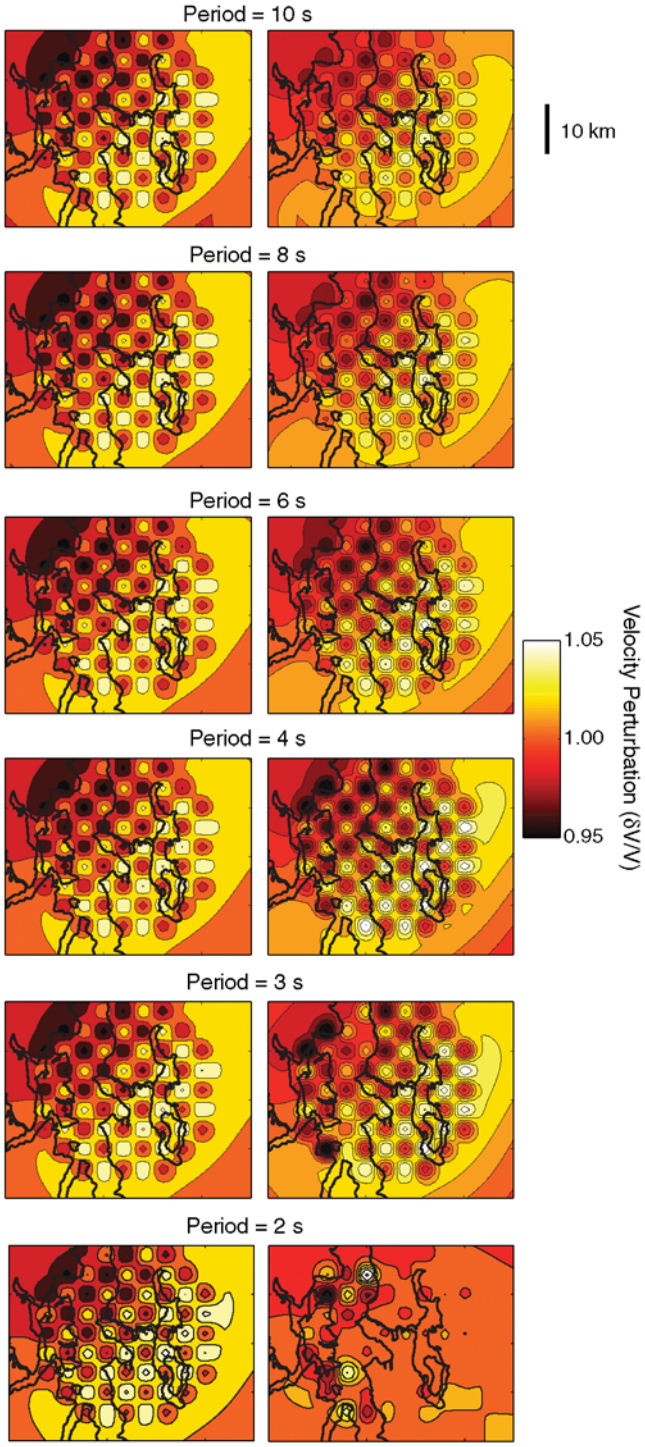

Figure 6. On the left is the synthetic model used to test the resolution of our dataset and on the right are the inversion results across four different periods. The color version of this figure is available only in the electronic edition.

of the synthetic model was very good at periods of 3 s and above and not very good at 2 s due to the limited number of paths used at this period. Vertical resolution is a little bit more difficult to assess because it depends upon the frequency range of the Rayleigh waves as well as path coverage and varies throughout the model. We do not, however, have the ability to resolve a feature as small as the potential velocity reversal beneath the hanging wall of the Seattle fault regardless of which fault model is assumed.

Results

Our Rayleigh-wave phase velocity results show a clear low-velocity zone that is consistent with the area of low isostatic residual gravity shown in Figure 1, measuring ~60 km from east to west and ~45 km from north to south (Fig. 7). The lowest velocities at all periods are near downtown Seattle, just to the north of the Seattle fault. Rayleigh waves with periods between 2 and 6 s are sensitive to the upper 5 km in this setting, and those with periods between 8 and 10 s are sensitive to the depth range 5–15 km. At a period of 2 s, the velocities are as low as ~625 m/s, and the lowest velocities at a period of 10 s are 960 m/s. With increasing period, the apparent diameter of the basin shrinks. Potential sub-basins are revealed in the southwest, north, and east. There is less apparent structure in the deeper parts of the basin. However, due to the broadening sensitivity kernels of Rayleigh waves at longer periods, it is also more difficult to resolve smaller structures with 8- to 10-s waves.

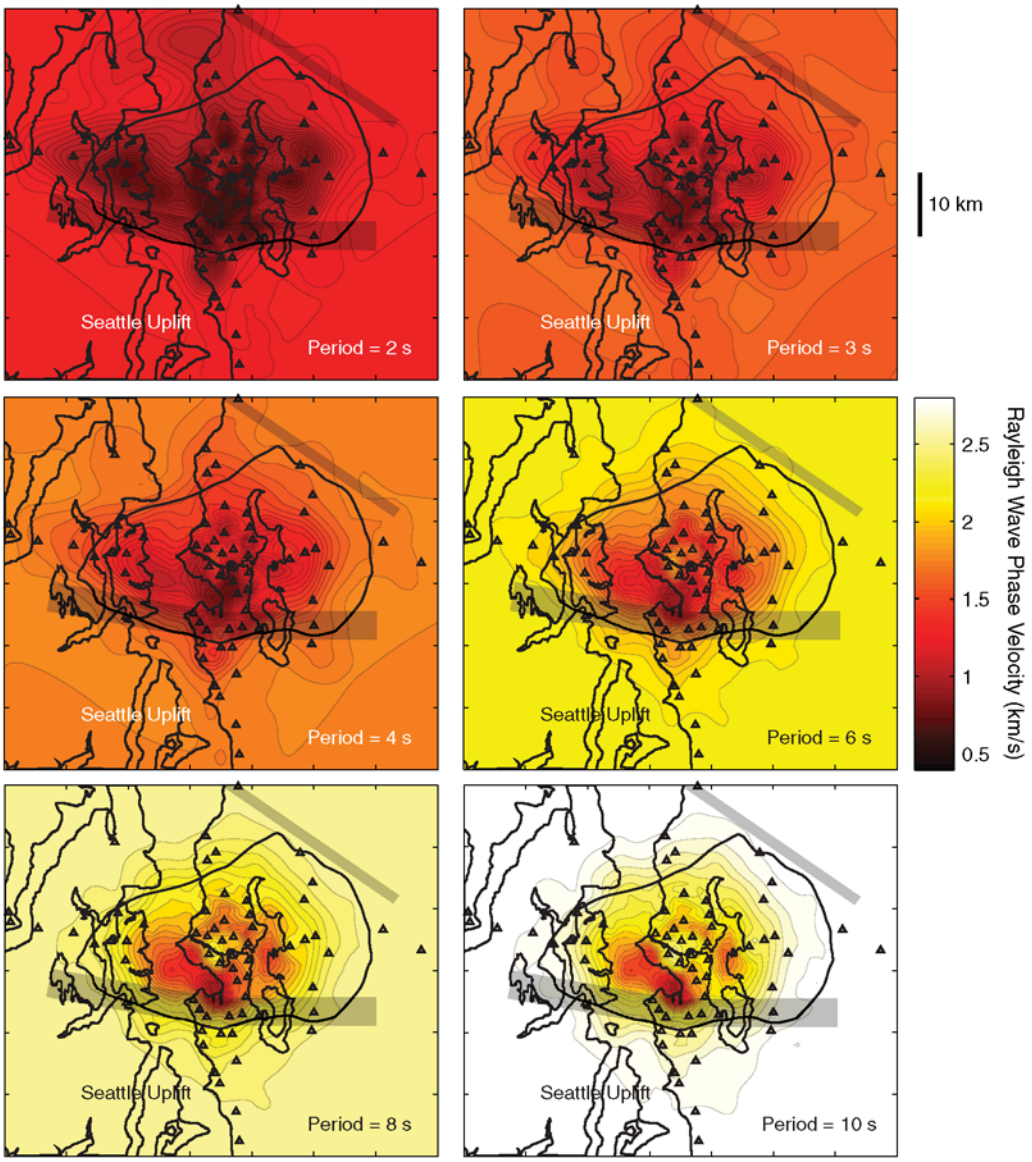

Figure 7. Rayleigh wave phase velocities for periods between 2 and 10 s. Black triangles represent stations of the 2002 SHIPS array. The upper gray patch indicates the location of the south Whidbey Island fault. The lower gray patch indicates the location of the Seattle fault zone. The closed curve indicates the approximate boundary of the Seattle basin based on the gravity measurements of Brocher *et al.* (2001). The color version of this figure is available only in the electronic edition.

Our V_S results show that velocities are slower in some areas in the top 1.5 km of the Seattle basin beneath the city of Seattle than in the model of Stephenson (2007; see Fig. 8). Additional images of our model and shear-wave velocities in table form are available as an Ⓔelectronic supplement to this paper. Our dataset does not uniquely constrain the uppermost ~250 m of the basin, but by using a 1D average from the model of Stephenson (2007) as our starting model, we inherit the ~600 m/s velocities in the uppermost layers from that model. By using different plausible starting models, the uppermost layer could be anywhere from 400–750 m/s according to our calculations. At 500 m and below, our calculations show little dependence on the starting model. Beneath the uppermost layers, we found that low velocities persist to at least 3 km, where our velocities were lowest just north of the Seattle fault with lesser amounts in other parts of the basin. Below 3 km, our results show velocities approaching those of Stephenson (2007).

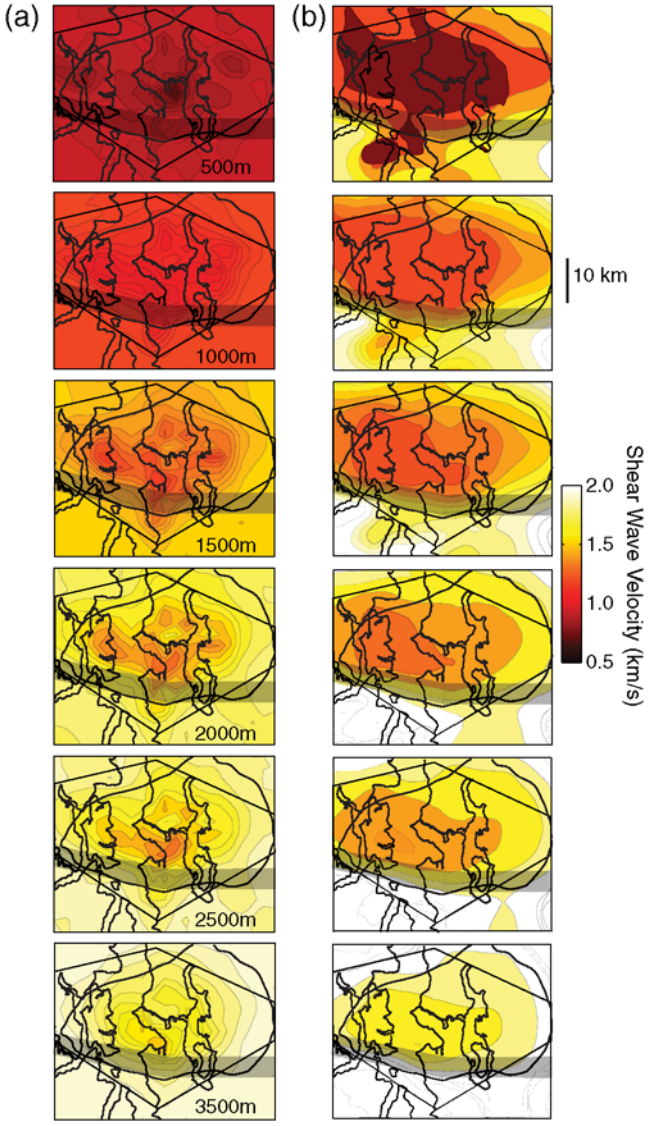

Figure 8. (a) Our V_S model and (b) the model of Stephenson (2007). Depths are indicated on each row. The gray patch indicates the location of the Seattle fault zone. The closed curve indicates the approximate boundary of the Seattle basin based the gravity measurements of Brocher *et al.*, (2001). The six-sided polygon represents the region of the model that is covered by our dataset. The color version of this figure is available only in the electronic edition.

We compared the 2D refraction profile of Snelson *et al.* (2007) that runs west to east across the Seattle basin to the same region from our new model. The Snelson *et al.* (2007) model has an origin at sea level and includes topography, while the origin of our model is the ground surface and does not include topography. If we align the top of the two models and look at the top 4 km where the models overlap, we can compare velocity contours. The biggest difference between the two models is that our model is a little slower in the top 1 km. To the west of Puget Sound, our model is slower throughout the top 4 km. Between Puget Sound and Lake Washington, our model is faster in the 1–3 km range then the two models that are very similar below 3 km. To the east of Lake Washington, our model is generally faster below 1 km. The Snelson *et al.*, (2007) model is missing contours beneath Puget Sound and Lake Washington due to a lack of ray paths, so we cannot compare these regions. A comparison of the two sets of contours is available as an Ⓔelectronic supplement to this paper.

Model Validation

We assessed our new model's ability to predict amplitudes in the 1- to 2-s range relative to the model of Stephenson (2007) because it was used in the development of Seattle's urban seismic-hazard map and because it was validated in this period range (Frankel *et al.*, 2009). There are other models we could have used for comparison; however, some of them are not tested at the shorter periods we address here (Pitarka *et al.*, 2004), while others are not well constrained in the shallowest parts of the basin (1.0–3.5 km) where our model is well constrained (Van Wagoner *et al.*, 2002) or are not 3D (Snelson *et al.*, 2007). Also, because other 3D V_S models are dependent on an accurate V_P/V_S ratio that is highly variable for sedimentary rocks (Brocher, 2005), it is hard to know if any differences between models are due to the tomography or to the V_P/V_S ratio. So, while the Stephenson (2007) model has similar limitations and is not necessarily the best overall model at the time of this report, it is the most relevant comparison in addressing our motive for improving seismic-hazard assessments.

For all of our amplitude comparisons, we calculated waveform envelopes. We calculated peak horizontal ground velocity (PGV) in a window that starts just before the direct shear-wave arrival and ends after the direct surface-wave arrival. We then took the geometric mean of the two horizontal components to capture both Love and Rayleigh waves and to eliminate any discrepancies with wave polarization. We used periods between 1 and 2 s because this is the shortest period band in which we think our model is valid. Also, it is

too computationally expensive to model shorter periods at this time. In this band was where we expected the most differences between the two models.

Frankel *et al.* (2009) showed a good phase match between data and synthetics for the 2001 Nisqually M_w 6.8 event in the 0.2- to 0.4-Hz band using the Stephenson (2007) model. We expected and produced very similar results in this band using our local model embedded in the Stephenson (2007) regional model because waves in this band are not strongly affected by updates to shallow structure from our tomography results. At the shorter periods addressed in this study, we neither expected nor achieved a good phase match between synthetics and data. We based our validation on the phase arrivals and velocity amplitudes of the shear and surface waves.

In Figure 9, we show an example of a data and synthetic time series for an earthquake recording to demonstrate what we considered a well-fitting prediction. Many of the urban strong motion sensors used in this study are by necessity located in noisy locations. Even though there is some noise in the data, the shear-wave and surface wave arrivals on the horizontal components are very close in arrival time and amplitude despite a phase mismatch. On the north component, the synthetic shear wave has higher amplitude than the data, but on the east component, that relationship is reversed. These differences could be the result of an issue with the modeled radiation pattern or unmodeled anisotropy as well as small inaccuracies in the velocity model. Because we use the geometric mean of both horizontal components and because the well-fitting surface wave controls the maximum amplitude in this example, the simulation yields an excellent match to the data. In addition, the amplitude of the coda is similar throughout this 50-s trace even though we did not consider the coda in our evaluation. In some other examples, one of the horizontal components fits well while the other one does not, or the arrival times are shifted slightly. Unmodeled scattering, focusing, and/or multipathing could explain some of these amplitude, phase, or arrival mismatches.

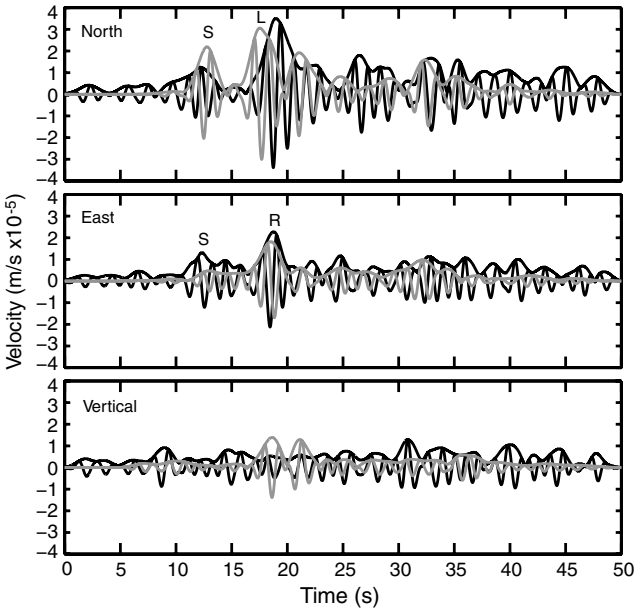

Figure 9. Velocity data and synthetic demonstrating goodness of fit. Data are shown in black, and synthetics are shown in gray. The shear-, Love-, and Rayleigh-wave arrivals are denoted with S, L, and R, respectively. Traces are bandpass filtered with corner frequencies of 0.5–1 Hz.

To evaluate the predictive ability of the two velocity models, we selected two local events that were widely recorded by strong-motion stations in the Seattle area, many of which were recently deployed. The first event, referred to hereafter as the Carnation event, had a coda duration magnitude (M_D) of 3.4 and occurred on 25 May 2010 at 47.679° N, −121.978° W (28 km east of Seattle) at a depth of 6 km (Fig. 10). This is a shallow crustal event with a hypocenter within the North American plate. The second event, referred to hereafter as the Kingston event, had an M_D of 4.5 and occurred on 30 January 2009 at 47.772° N, 122.557° W (25 km northwest of Seattle) at a depth of 58 km (Fig. 11). This is a Wadati–Benioff zone event with a hypocenter located within the subducting Juan de Fuca plate. Event locations and magnitudes are obtained from the PNSN catalog. We used the finite-difference code of Liu and Archuleta (2002) to simulate these two earthquakes for comparison with the recorded data.

Because neither of the two local events had a hypocenter within our new model, we embedded our new model into the regional model of Stephenson (2007), which encompasses both hypocenter locations. We extracted the upper 3.5 km of our new model and pasted it into the model of Stephenson (2007). We applied some averaging near the suture between the two models to avoid discontinuities and then explicitly added a discontinuity to represent the Seattle fault. This fault discontinuity follows the frontal surface trace described by Blakely *et al.* (2002), dips 45° to the south, and is given a 10% velocity contrast that decays exponentially away from the fault surface.

Vertically propagating shear waves at periods greater than 3 s in a medium with velocities between 600 and 1500 m/s will not be strongly affected by a 3.5-km thick section, the maximum depth of our new velocity model within the regional velocity model. Body and surface waves at periods between 1 and 2 s can be strongly affected by a 3.5-km thick region. We expected and observed that long-period (> 3 s) arrivals calculated using the two models would be very similar to one another in phase and amplitude, while shorter period waves would be often different.

The Carnation event was recorded on 27 stations located on stiff soil sites as shown in Figure 10a. For 15 of these stations, amplitudes at periods between 1 and 2 s, calculated using our new model are closer to the data by more than 5% when compared to amplitudes using the previous model. For two of these stations, there is less than 5% difference between the two models. For 10 stations, the previous model yields more accurate amplitude predictions by more than 5%.

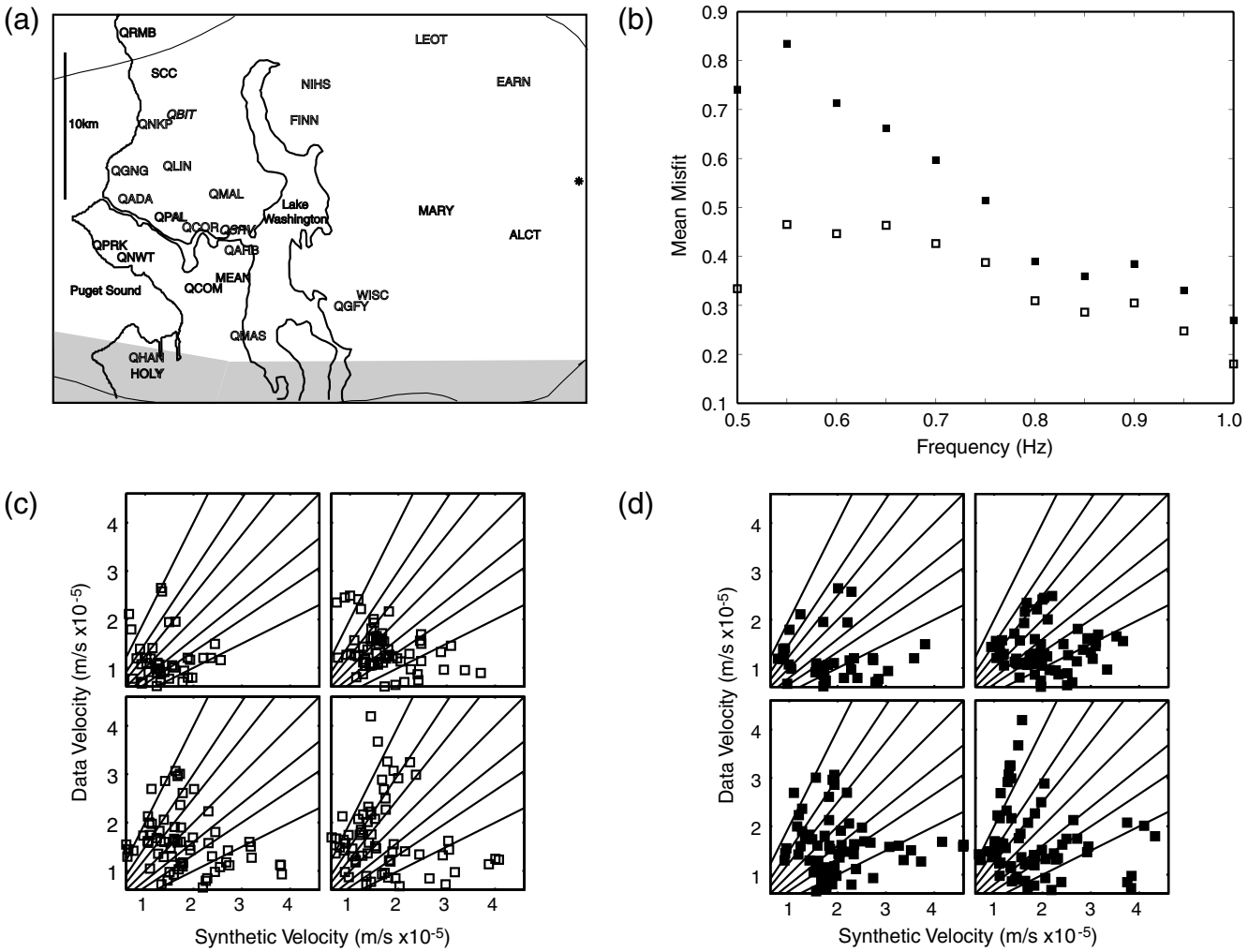

Figure 10. Carnation event. (a) The asterisk indicates the event epicenter. Outlined station names indicate stations where our new model produces better PGVs than the previous model. Bold station names indicate stations where the previous model produces better PGVs than our new model. Italicized station names indicate stations where PGVs produced by the two models are within 5%. (b) The average misfit as a function of frequency is shown. Solid squares indicate PGV misfit for the previous model, and open squares indicate PGV misfit for our new model. Scatter plot for PGVs for all stations and all frequencies shown in (a) and (b) calculated from (c) our new model, and (d) the previous model compared to the observed amplitudes in four equally-sized bins between 0.5 and 1 Hz are shown from left to right then top to bottom. In these four axes, when a square is on the center line with a slope of one, that indicates a perfect match of PGVs between data and synthetic. The next line with a smaller slope indicates that the synthetic is 25% greater than the data. The next two lines with smaller slopes indicate 50% and 100% greater, respectively. The lines with a slope greater than one indicate $1/1.25$, $1/1.5$, and $1/2$, respectively, with the data greater than the synthetic. The black curve, only partially shown, indicates the approximate boundary of the Seattle basin based on the gravity measurements of Brocher *et al.* (2001), and the gray patch indicates the location of the Seattle fault zone.

We also averaged the misfit across all stations at different frequencies between 0.5 and 1 Hz (Fig. 10b). We calculated the points on this figure by first dividing the synthetic amplitude by the data amplitude. Then we subtracted one from the absolute value of the mean ratio for each station so that a value of zero indicates a perfect match in amplitude. Average amplitudes calculated using our new model are closer to the data than those calculated using the previous model at all frequencies in the range. Even though the previous model makes better predictions at some stations, the difference between the two models tends to be smaller at those stations than for stations where our new model does better, which is evident in the averages shown in Figure 10b.

In Figure 10c,d, we show a scatter plot of the amplitudes for all stations and all frequencies that are averaged to make Figure 10b. There is a significant amount of scatter that could represent either site effects from unconsolidated sediments or unmodeled structure. As a local crustal event, the seismic waves traveling from the hypocenter to each station travel ~20 km through heterogeneous upper crust. We will see that the Kingston event, a Wadati–Benioff zone earthquake, has a much tighter scatter plot due to fewer path effects.

In addition to the complications due to path effects, there is some uncertainty in the M_w for the Carnation event, which we initially assumed was equivalent to the M_D 3.4 from the PNSN catalog. Using an M_w 3.4 results in the amplitudes of

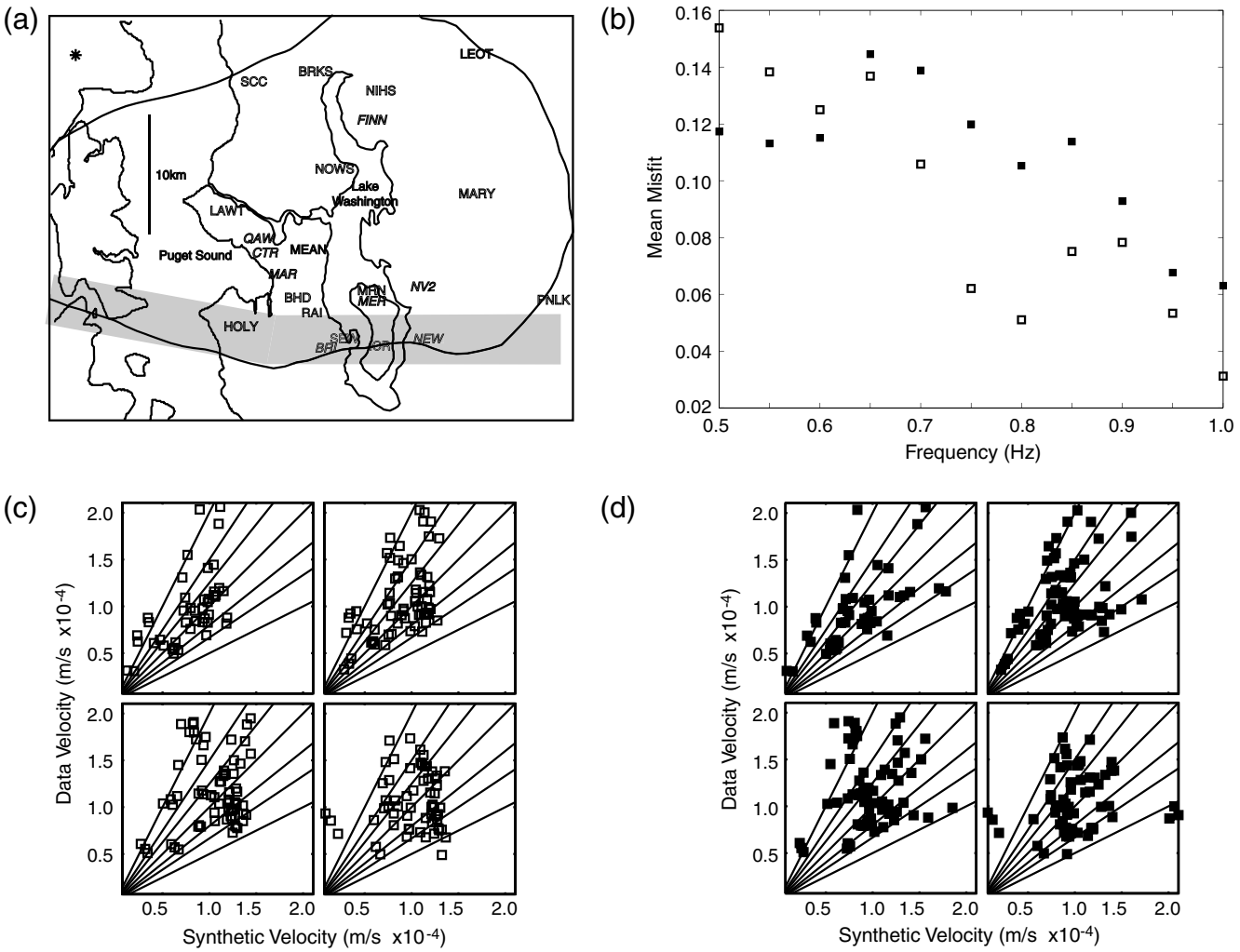

Figure 11. Kingston event. (a) The asterisk indicates the event epicenter. Outlined station names indicate stations where our new model produces better PGVs than the previous model. Bold station names indicate stations where the previous model produces better PGVs than our new model. Italicized station names indicate stations where PGVs produced by the two models are within 5%. (b) The average misfit as a function of frequency is shown. Solid squares indicate PGV misfit for the previous model, and open squares indicate PGV misfit for our new model. Scatter plot for PGVs for all stations and all frequencies shown in (a) and (b) calculated from (c) our new model and (d) the previous model compared to the observed amplitudes in four equally-sized bins between 0.5 and 1 Hz are shown from left to right then top to bottom. In these four axes, when a square is on the center line with a slope of one, that indicates a perfect match of PGVs between data and synthetic. The next line with a smaller slope indicates that the synthetic is 25% greater than the data. The next two lines with smaller slopes indicate 50% and 100% greater, respectively. The lines with a slope greater than one indicate $1/1.25$, $1/1.5$, and $1/2$, respectively, with the data greater than the synthetic. The black curve, only partially shown, indicates the approximate boundary of the Seattle basin based on the gravity measurements of Brocher *et al.* (2001), and the gray patch indicates the location of the Seattle fault zone.

the synthetics systematically overestimating the amplitudes of the data using both models. We found that simulating this event with an M_w 3.25 resulted in the best overall fit of our model with the data. Amplitudes calculated with our new model are more closely clustered around the observed amplitudes, especially at longer periods in the range considered using this M_w. In order to adjust the M_w to best fit the results from the previous model, the M_w would have to be less than M_w 3.25.

The Kingston event was recorded by 23 stations located on stiff soil sites as shown in Figure 11a. For 12 of these stations, amplitudes calculated using our new model are closer to the data by more than 5% as compared to amplitudes using the previous model. For eight of these stations, there is less than 5% difference between the two models. For three stations, the previous model yields more accurate amplitude predictions by more than 5%. We also averaged the misfit across all stations at different frequencies between 0.5–1 Hz (Fig. 11b). Between periods of 1.0–1.67 s, our new model has amplitudes closer to the data, while the previous model has better amplitudes between 1.67 and 2.0 s. Compared to the Carnation event, synthetic amplitudes are a closer match to the data amplitudes for both models; however, our new model makes better predictions at most

of the individual stations. In Figure 11c,d, we show a scatter plot of the amplitudes for all stations and all frequencies that are averaged to make Figure 11b.

Overall, the improvement of our predictions over the predictions made with the previous model for the Kingston event is smaller than for the Carnation event. Because the Kingston event is almost directly below the Seattle basin and is at a depth of almost 60 km, most of the wave path is in the mantle with only the top 3.5 km different in the two models. For the Carnation event, which is a shallow crustal event, most of the wave path is in the crust, and waves travel horizontally through our model for distances much greater than 3.5 km, so our model will have a greater impact on the predictions made from shallow events.

Discussion

Because we have observed that the Seattle basin can amplify both surface waves (Barberopoulou *et al.*, 2004) and body waves (Frankel *et al.*, 2002), the cause of the amplification is likely to be in the upper crust. There are two likely explanations: the observed amplification is produced by the velocity contrast between basin sediments and the surrounding rock, or it is produced by the site response of shallow unconsolidated sediments. Because amplifications are observed in a variety of soil conditions (Frankel *et al.*, 2002; Pratt, Brocher, *et al.*, 2003; Barberopoulou *et al.*, 2004; Stephenson *et al.*, 2006; Frankel *et al.*, 2009), the amplifications are likely caused, at least in part, by the velocity contrast between basin sediments and the surrounding rock. However, we expect that the velocity contrast is the largest in the top few kilometers due to increasing compaction of basin sediments with depth. In order for a velocity model to be useful in predicting how the Seattle basin produces the observed amplifications, V_S must be well understood in the top few kilometers.

There are two major deficiencies in previous Seattle-basin velocity models regarding their usefulness for predicting ground motions: (1) all previous 3D V_S models were produced by measuring V_P and using an uncertain V_P/V_S relationship to determine V_S; our model is based on direct observations of V_S, and (2) all previous models are either poorly resolved in the upper 4 km or are produced by interpolating across a sparsely sampled model space when considered on the scale of the Seattle basin; our model is well sampled horizontally throughout the Seattle basin and best resolved in the top 3.5 km. Tomography, using either active-source or passive-source body-wave travel times, yields very little constraint on velocities in the upper 4 km because body waves are nearly vertically propagating near the surface and because ray paths are clustered around the recording stations (Van Wagoner *et al.*, 2002; Pitarka *et al.*, 2004; Ramachandran *et al.*, 2006). The precise depth of velocity perturbations is unknown due to the vertically oriented ray paths and observations that must be interpolated in a horizontal sense because the ray paths cluster beneath the recording stations. Body-wave studies using the SHIPS dataset with both active and passive sources yield a horizontal resolution of 10–15 km (Van Wagoner *et al.*, 2002; Ramachandran *et al.*, 2006) and vertical resolution on the order of 5 km, much more coarse than our model (~4 km horizontal) and not very useful for making high-frequency (~1 Hz) predictions for ground motions within the Seattle basin. Our entire model would be a single pixel in depth and just a few pixels horizontally in the resolution tests of the other models.

At the other end of the model scale, our model does not include information about shallow, unconsolidated sediments, topography, or nonlinear response. These issues must be considered additionally to have a complete accounting of the inputs to ground motion. However, this study fills a gap in our knowledge between regional velocity models (Van Wagoner *et al.*, 2002; Pitarka *et al.*, 2004; Ramachandran *et al.*, 2006; Stephenson, 2007) and local site response studies (Hartzell *et al.*, 2000). The appropriate evaluation for our new model is to compare ground-motion predictions made by our new model to predictions made to produce Seattle's urban seismic-hazard map (Frankel *et al.*, 2007), rather than to compare it to the aforementioned regional velocity models.

According to our resolution test, we are able to resolve structures within the Seattle basin on the order of 4 km or less in length horizontally and velocity contrasts across discrete geologic features like the Seattle fault. There is a pronounced low-velocity zone just north of the Seattle fault in Elliot Bay at the outlet of the Duwamish river, which is most evident at 1-km depth (Fig. 8). Basin sediments have lower velocities than the mostly crystalline rock to the south and north, and we are able to resolve this contrast. To the west across Puget Sound, the fault trace shifts northward (Blakely *et al.*, 2002), which can be seen in our model at depths from 1–3 km (Fig. 8). Our data do not cover the entire length of the Seattle fault, but in places where we have data coverage, we observed the associated velocity contrast. Velocity variations within the basin reveal several sub-basins that could have at least two different origins. Deeper sub-basins are likely formed by the evolution of the basin through a combination of thrust and strike-slip tectonic motions, while shallower sub-basins are likely the result of glacial action including uneven compaction, deposition, and erosion.

Conclusions

The 3D V_S structure of deep crustal basins has a significant impact on the propagation of seismic waves and seismic hazards in the cities that sit atop them. We used Rayleigh waves extracted from ambient noise with periods between 2 and 10 s to directly observe the V_S structure of the Seattle basin, avoiding the use of uncertain V_P/V_S ratios. Unlike body waves, short-period surface waves can resolve structure in the upper ~4 km with enough detail to model

high-frequency (1 Hz) strong motions in regions with upper crustal structures like the Seattle basin.

Our method's strength is the resolving power of short-period Rayleigh waves on V_S in the upper few kilometers without the need to precisely know Poisson's ratio. This is precisely the region where many previous models are least well constrained. We believe that our new model can be applied to predict levels of ground shaking with greater accuracy than the current urban seismic-hazard maps for Seattle (Frankel *et al.*, 2007), as demonstrated by the two events we examined, due to more accurate modeling of V_S in the upper 3–4 km of the basin.

We believe that most of the remaining misfit is likely due the effect of shallow, unconsolidated sediments, features smaller than a few kilometers, and unmodeled structure from outside our area of data coverage. The weaknesses of this dataset are its inability to precisely resolve sharp discontinuities and uniquely constrain velocities in the top 250 m. With a richer dataset, we believe these weaknesses could be overcome using our method.

Further improvements in the Seattle-basin velocity model could be achieved using a more optimal station arrangement, more broadband instruments, a longer recording duration, and developing a joint inversion that explicitly includes geological information about sharp discontinuities such as faults and basin edges. However, using a limited, legacy dataset we were able to demonstrate the usefulness of this method by making measurable improvements to amplitude predictions for two local earthquakes at frequencies relevant to seismic-hazard assessments.

Data and Resources

This study uses data collected during the SHIPS 2002 experiment, which was obtained from the IRIS Data Management Center. This study also uses data collected by Earthscope's Transportable Array (TA) and the Pacific Northwest Seismic Network (PNSN), also available from the IRIS Data Management Center.

Acknowledgments

The authors wish to acknowledge Tom Pratt for his assistance in analyzing the SHIPS 2002 dataset and Art Frankel for consultations regarding the Seattle basin and seismic hazards. The authors also wish to acknowledge several reviewers for their feedback: Tom Pratt, Catherine Snelson, Ivan Wong, and an anonymous reviewer.

References

Atwater, B. F. (1992). Geologic evidence for earthquakes during the past 2000 years along the Copalis River, southern coastal Washington, *J. Geophys. Res.* **97,** 1901–1919, doi 10.1029/91JB02346.

Barberopoulou, A., A. Qamar, T. L. Pratt, K. C. Creager, and W. P. Steele (2004). Local amplification of seismic waves from the Denali earthquake and damaging seiches in Lake Union, Seattle, Washington, *Geophys. Res. Lett.* **31,** L03607, doi 10.1029/2003GL08569.

Bensen, G. D., M. H. Ritzwoller, M. P. Barmin, A. L. Levshin, F. Lin, M. P. Moschetti, N. M. Shapiro, and Y. Yang (2007). Processing seismic ambient noise data to obtain reliable broad-band surface wave dispersion measurements, *Geophys. J. Int.* **169,** 1239–1260, doi 10.1111/j.1365-246X.2007.03374.x.

Blakely, R. J., R. E. Wells, C. S. Weaver, and S. Y. Johnson (2002). Location, structure, and seismicity of the Seattle fault zone, Washington: Evidence from aeromagnetic anomalies, geologic mapping, and seismic-reflection data, *Bull. Geol. Soc. Am.* **114,** 169–177.

Booth, D. B. (1994). Glaciofluvial infilling and scour of the Puget lowland, Washington, during ice-sheet glaciation, *Geology* **22,** 695–698, doi 10.1130/0091-7613(1994)022<0695:GIASOT>2.3.CO;2.

Brocher, T. M. (2005). Empirical relations between elastic wavespeeds and density in the Earth's crust, *Bull. Seismol. Soc. Am.* **95,** 2081–2092, doi 10.1785/0120050077.

Brocher, T. M., R. J. Blakely, and R. E. Wells (2004). Interpretation of the Seattle uplift, Washington, as a passive roof duplex, *Bull. Seismol. Soc. Am.* **94,** 1379–1401.

Brocher, T. M., T. E. Parsons, R. J. Blakely, N. I. Christensen, M. A. Fisher, R. E. Wells, U. S. ten Brink, T. L. Pratt, R. S. Crosson, K. C. Creager, N. P. Symons, L. A. Preston, T. Van Wagoner, K. C. Miller, C. M. Snelson, A. M. Trehu, V. E. Langenheim, G. D. Spence, K. Ramachandran, R. D. Hyndman, D. C. Mosher, B. C. Zelt, and C. S. Weaver (2001). Upper crustal structure in Puget lowland, Washington: Results from the 1998 seismic hazards investigation in Puget Sound, *J. Geophys. Res.* **106,** 13541–13564.

Bucknam, R. C., E. Hemphill-Haley, and E. B. Leopold (1992). Abrupt uplift within the past 1700 years at southern Puget Sound, Washington, *Science* **258,** 1611–1614.

Frankel, A. D., D. L. Carver, E. Cranswick, M. E. Meremonte, T. Bice, and D. E. Overturf (1999). Site response for Seattle and source parameters of earthquakes in the Puget Sound region, *Bull. Seismol. Soc. Am.* **89,** 468–483.

Frankel, A. D., D. L. Carver, and R. A. Williams (2002). Nonlinear and linear site response and basin effects in Seattle for the *M* 6.8 Nisqually, Washington, earthquake, *Bull. Seismol. Soc. Am.* **92,** 2090–2109.

Frankel, A. D., C. Mueller, T. Barnhard, D. Perkins, E. V. Leyendecker, N. Dickman, S. Hanson, and M. Hopper (1996). National seismic-hazard maps: Documentation June 1996, *U.S. Geol. Surv. Open-File Rept.* 96–532, 69 pp.

Frankel, A. D., W. J. Stephenson, and D. Carver (2009). Sedimentary basin effects in Seattle, Washington: Ground-motion observations and 3D simulations, *Bull. Seismol. Soc. Am.* **99,** 1579–1611, doi 10.1785/0120080203.

Frankel, A. D., W. J. Stephenson, D. L. Carver, R. A. Williams, J. K. Odum, and S. Rhea (2007). Seismic hazard maps for Seattle, Washington, incorporating 3D sedimentary basin effects, nonlinear site response, and rupture directivity, *U.S. Geol. Surv. Open-File Rept. 07-1175* 77 pp., 3 plates.

Goldfinger, C., C. H. Nelson, and J. E. Johnson (2003). Deep-water turbidites as Holocene earthquake proxies: the Cascadia subduction zone and northern San Andreas fault systems, *Ann. Geophys.* **46,** 1169–1194.

Hartzell, S., D. Carver, E. Cranswick, and A. D. Frankel (2000). Variability of site response in Seattle, Washington, *Bull. Seismol. Soc. Am.* **90,** 1237–1250.

Haugerud, R. A., D. J. Harding, S. Y. Johnson, J. L. Harless, C. S. Weaver, and B. L. Sherrod (2003). High-resolution lidar topography of the Puget lowland, Washington, *GSA Today* **13,** 4–10.

Ichinose, G. A., H. K. Thio, and P. G. Somerville (2004). Rupture process and near-source shaking of the 1965 Seattle-Tacoma and 2001 Nisqually, intraslab earthquakes, *Geophys. Res. Lett.* **31,** L10604, doi 10.1029/2004GL019668.

Ichinose, G. A., H. K. Thio, and P. G. Somerville (2006). Moment tensor and rupture model for the 1949 Olympia, Washington, earthquake and scaling relations for Cascadia and global intraslab earthquakes, *Bull. Seismol. Soc. Am.* **96,** 1029–1037, doi 10.1785/0120050132.

Johnson, S. Y., C. J. Potter, J. M. Armentrout, J. J. Miller, C. A. Finn, and C. S. Weaver (1996). The southern Whidbey Island fault: An active

structure in the Puget lowland, Washington, *Bull. Geol. Soc. Am.* **108,** 334–354, doi 10.1130/0016-7606(1996)108<0334:TSWIFA>2.3.CO;2.

Lees, J. M., and R. S. Crosson (1990). Tomographic imaging of local earthquake delay times for 3-dimensional velocity variation in Western Washington, *J. Geophys. Res.* **95,** 4763–4776, doi 10.1029/JB095iB04p04763.

Li, Q., W. S. D. Wilcock, T. L. Pratt, C. M. Snelson, and T. M. Brocher (2006). Seismic attenuation structure of the Seattle basin, Washington State, from explosive-source refraction data, *Bull. Seismol. Soc. Am.* **96,** 553–571, doi 10.1785/0120040164.

Liu, P. C., and R. J. Archuleta (2002). The effect of a low-velocity surface layer on simulated ground motion, *Seismol. Res. Lett* **73,** 267.

Pitarka, A., R. Graves, and P. Somerville (2004). Validation of a 3D model of the Puget Sound region based on modeling ground motion from the 28 February 2001 Nisqually earthquake, *Bull. Seismol. Soc. Am.* **94,** 1670–1689.

Pratt, T. L., T. M. Brocher, C. S. Weaver, K. C. Creager, C. M. Snelson, R. S. Crosson, K. C. Miller, and A. M. Trehu (2003). Amplification of seismic waves by the Seattle basin, Washington State, *Bull. Seismol. Soc. Am.* **93,** 533–545.

Pratt, T. L., S. Y. Johnson, C. J. Potter, W. J. Stephenson, and C. A. Finn (1997). Seismic reflection images beneath Puget Sound, western Washington State: The Puget lowland thrust sheet hypothesis, *J. Geophys. Res.* **102,** 27,469–427,489, doi 10.1029/97JB01830.

Pratt, T. L., K. L. Meagher, T. M. Brocher, T. Yelin, R. D. Norris, L. Hultgrien, E. A. Barnett, and C. S. Weaver (2003). Earthquake recordings from the 2002 Seattle Seismic Hazard Investigation of Puget Sound (SHIPS), Washington State, *U.S. Geol. Surv. Open-File Rept. 03-361*, 72 pp.

Ramachandran, K., S. E. Dosso, G. D. Spence, R. D. Hyndman, and T. M. Brocher (2005). Forearc structure beneath southwestern British Columbia: A 3-D tomography velocity model, *J. Geophys. Res.* **110,** B02303, doi 10.1029/2004JB003258.

Ramachandran, K., S. E. Dosso, C. A. Zelt, G. D. Spence, R. D. Hyndman, and T. M. Brocher (2004). Upper crustal structure of southwestern British Columbia from the 1998 Seismic Hazards Investigation in Puget Sound, *J. Geophys. Res.* **109,** B09303, doi 10.1029/2003JB002826.

Ramachandran, K., R. D. Hyndman, and T. M. Brocher (2006). Regional *P* wave velocity structure of the Northern Cascadia subduction zone, *J. Geophys. Res.* **111,** B12301, doi 10.1029/2005JB004108.

Riddihough, R. P. (1984). Recent movements of the Juan de Fuca plate system, *J. Geophys. Res.* **89,** 6980–6994, doi 10.1029/JB089iB08p06980.

Satake, K., K. Wang, and B. F. Atwater (2003). Fault slip and seismic moment of the 1700 Cascadia earthquake inferred from Japanese tsunami descriptions, *J. Geophys. Res.* **108,** 2535, doi 10.1029/2003JB002521.

Schultz, A. P., and R. S. Crosson (1996). Seismic velocity structure across the central Washington Cascade Range from refraction interpretation with earthquake sources, *J. Geophys. Res.* **101,** 27899–27915, doi 10.1029/96JB02289.

Sherrod, B. L., T. M. Brocher, C. S. Weaver, R. C. Bucknam, R. J. Blakely, H. M. Kelsey, A. R. Nelson, and R. Haugerud (2004). Holocene fault scarps near Tacoma, Washington, USA, *Geology* **32,** 9–12, doi 10.1130/G19914.1.

Snelson, C. M., T. M. Brocher, K. C. Miller, T. L. Pratt, and A. M. Trehu (2007). Seismic amplification within the Seattle basin, Washington state: Insights from SHIPS seismic tomography experiments, *Bull. Seismol. Soc. Am.* **97,** 1432–1448, doi 10.1785/0120050204.

Stephenson, W. J. (2007). Velocity and density models incorporating the Cascadia subduction zone for 3D earthquake ground motion simulation, *U.S. Geol. Surv. Open-File Rept. 07-1348*, 24 pp.

Stephenson, W. J., A. Frankel, J. K. Odum, R. A. Williams, and T. L. Pratt (2006). Towards resolving an earthquake ground motion mystery in west Seattle, Washington state: Shallow seismic focusing may cause anomalous chimney damage, *Geophys. Res. Lett.* **33,** L06316, doi 10.1029/2005GL025037.

Symons, N. P., and R. S. Crosson (1997). Seismic velocity structure of the Puget Sound region from 3-D non-linear tomography, *Geophys. Res. Lett.* **24,** 2593–2596, doi 10.1029/97GL52692.

Takeuchi, H., and M. Saito (1972). Seismic surface waves, in *Methods in Computational Physics*, B. A. Bolt (Editor), Vol. 11, Academic Press, New York, pp. 217–195.

ten Brink, S. U., P. C. Molzer, M. A. Fisher, R. J. Blakely, R. C. Bucknam, T. Parsons, R. S. Crosson, and K. C. Creager (2002). Subsurface geometry and evolution of the Seattle fault zone and the Seattle Basin, Washington, *Bull. Seismol. Soc. Am.* **92,** 1737–1753.

ten Brink, S. U., J. Song, and R. C. Bucknam (2006). Rupture models for the A.D. 900-930 Seattle Fault earthquake from uplifted shorelines, *Geology* **34,** 585–588.

Van Wagoner, T. M., R. S. Crosson, K. C. Creager, G. F. Medema, L. A. Preston, N. P. Symons, and T. M. Brocher (2002). Crustal structure and relocated earthquakes in the Puget lowland, Washington, from high-resolution seismic tomography, *J. Geophys. Res.* **107,** 2381, doi 10.1029/2001JB000710.

Wells, R. E., and R. W. Simpson (2001). Northward migration of the Cascadia forearc in the northwestern U.S. and implications for subduction deformation, *Earth Planets Space* **53,** 275–283.

Wells, R. E., C. S. Weaver, and R. J. Blakely (1998). Fore-arc migration in Cascadia and its neotectonic significance, *Geology* **26,** 759–762, doi 10.1130/0091-7613(1998)026<0759:FAMICA>2.3.CO;2.

Department of Earth and Space Sciences
University of Washington
Johnson Hall Rm-070, Box 351310
4000 15th Avenue NE
Seattle, Washington 98195-1310

Manuscript received 23 September 2010